ASRL TR 153-1

LEADING-EDGE PRESSURE MEASUREMENTS OF AIRFOIL VORTEX INTERACTION

Robert G. Walsh, Jr.

MASSACHUSETTS INSTITUTE OF TECHNOLOGY
AEROELASTIC AND STRUCTURES RESEARCH LABORATORY
CAMBRIDGE, MASSACHUSETTS 02139

January 1970

(NASA-CR-112129) LEADING-EDGE PRESSURE MEASUREMENTS OF AIRFOIL VORTEX INTERACTION R.G. Walsh, Jr. (Massachusetts Inst. of Tech.) Jan. 1970 34 p CSCL 20D

N72-29226

G3/12 Unclas 15666

NASA-LANGLEY SPACE RESEARCH CENTER
GRANT NUMBER NGR-22-009-303

Reproduced by
NATIONAL TECHNICAL INFORMATION SERVICE
U.S Department of Commerce
Springfield VA 22151

ASRL TR 153-1

LEADING-EDGE PRESSURE MEASUREMENTS OF AIRFOIL VORTEX INTERACTION

Robert G. Walsh, Jr.

Massachusetts Institute of Technology
Aeroelastic and Structures Research Laboratory

January 1970

This document has been approved for public release and sale; its distribution is unlimited.

Prepared for

NASA-Langley Space Research Center

Grant Number NGR-22-009-303

Rgt-65718

FOREWORD

This report was prepared by the Aeroelastic and Structures Research Laboratory, Department of Aeronautics and Astronautics, Massachusetts Institute of Technology, Cambridge, Massachusetts, under NASA Grant No. NGR 22-009-(303)

This report is unclassified.

UNCLASSIFIED
Security Classification

DOCUMENT CONTROL DATA - R & D

(Security classification of title, body of abstract and indexing annotation must be entered when the overall report is classified)

1. ORIGINATING ACTIVITY (Corporate author) Massachusetts Institute of Technology Aeroelastic & Structures Research Lab. Cambridge, Massachusetts	2a. REPORT SECURITY CLASSIFICATION Unclassified 2b. GROUP

3. REPORT TITLE
Leading-Edge Pressure Measurements of Airfoil Vortex Interaction

4. DESCRIPTIVE NOTES (Type of report and inclusive dates)
Technical Report

5. AUTHOR(S) (First name, middle initial, last name)
Robert G. Walsh, Jr.

6. REPORT DATE	7a. TOTAL NO. OF PAGES	7b. NO. OF REFS
January 1970	29	8

8a. CONTRACT OR GRANT NO.	9a. ORIGINATOR'S REPORT NUMBER(S)
NGR-22-009-303 b. PROJECT NO	ASRL TR 153-1
c.	9b. OTHER REPORT NO(S) (Any other numbers that may be assigned this report)
d.	

10. DISTRIBUTION STATEMENT
This document has been approved for public release and sale; its distribution is unlimited.

11. SUPPLEMENTARY NOTES	12. SPONSORING MILITARY ACTIVITY
	NASA-Langley Space Research Center

13. ABSTRACT

This report presents experimental pressure-differential measurements made at 10% chord of an airfoil-vortex interaction. A line vortex was oscillated over an airfoil perpendicular to the span and parallel to the chord. The pressure time history was recorded in order to show the sharp pressure pulses resulting from the bursting of the vortex core as it impinges upon the airfoil. Results for various vortex sizes and free-stream velocities were obtained. Measurements were also made when the airfoil was yawed to the line vortex. Maximum pressure differences were observed to occur in phase across the blade even with yaw, and were directly proportional to the square of the free-stream velocity. The maximum dynamic pressures obtained values as high as 1.0 when vortex bursting occurred.

DD FORM 1 NOV 65 1473

UNCLASSIFIED
Security Classification

14 KEY WORDS	LINK A		LINK B		LINK C	
	ROLE	WT	ROLE	WT	ROLE	WT
Helicopter Noise						
Blade Slap						
Airfoil-Vortex Interaction						
Vortex Bursting						
Airfoil Tip Vorticity						
Vortex Rollup						

ABSTRACT

This report presents experimental pressure-differential measurements made at 10% chord of an airfoil-vortex interaction. A line vortex was oscillated over an airfoil perpendicular to the span and parallel to the chord. The pressure time history was recorded in order to show the sharp pressure pulses resulting from the bursting of the vortex core as it impinges upon the airfoil. Results for various vortex sizes and free-stream velocities were obtained. Measurements were also made when the airfoil was yawed to the line vortex. Maximum pressure differences were observed to occur in phase across the blade even with yaw, and were directly proportional to the square of the free-stream velocity. The maximum dynamic pressure coefficients obtained were as high as 1.0 when vortex bursting occurred.

CONTENTS

SYMBOLS

c	Chord of airfoil
f	Vorticity in cycles/second
Hz	Frequency in cycles per second
$\Delta p(t)$	Unsteady pressure differential at 10% chord
r	Radius of axisymmetric vortex
T.E.	Offset of trailing edge from tunnel centerline of oscillating upstream airfoil
U	Free-stream velocity, tunnel air speed
$u(r)$	Induced velocity of vortex
p	Dynamic or stagnation pressure = $1/2\rho u^2(t)$
y	Spanwise coordinate
+, -	Sign of angles of attack of upstream oscillating airfoil
α	Angle of attack of upstream oscillating airfoil
Γ	Total circulation of vortex
ρ	Density of air
ν	Kinetic viscosity of air
ζ	Vorticity in radians/second
$\frac{\Delta p(t)}{\frac{1}{2}\rho U^2}$	Dynamic pressure coefficient

Introduction

This investigation is an initial experimental step into the noise problem resulting from rotary wing aircraft. Harmonic analysis of the blade loading in such operations has not successfully shown, nor is able to estimate, the loading and thus the noise at high frequencies (greater than approximately 20 blade harmonics [Ref. 1]). Rotor noise has been classified into three basic groups [Ref. 2], which are rotational noise, as described above, vortex noise, and blade slap. The vortex noise is actually the result of turbulent flow caused by boundary-layer separation, vortex shedding, and the operation of airfoils in a turbulent wake. Blade slap is a characteristic impulsive sound which occurs when strong interaction occurs between a blade and a trailing vortex or when a blade tip experiences strong compressibility effects, usually over a portion of a cycle.

This report is concerned only with the problem of blade slap caused by vortex interaction. Reference 3 presents an approach to the vortex interaction noise problem, which will be considered later in this report. The result of measuring the unsteady pressure forces caused by vortex interaction (both magnitude and phase along the span of the blade) will not only yield the unsteady blade load, but will also indicate the intensity of dipole-type noise expected to be radiated from the blades. The theoretical understanding of this phenomena is given in Ref. 5. This procedure of determining the acoustic dipole strength is the method used in Ref. 1 for estimating the radiated noise from the overall harmonic blade loading.

Examination of the most simplified relevant two-dimensional problem consists of a two-dimensional airfoil having a free space, line vortex passing near and over the blade. See Fig. 1. If the vortex does not pass over the airfoil, estimates of the varying lift due to the vortex may be calculated using methods given in Ref. 4 which are based on potential flow theory. However, when the vortex

passes across the airfoil, vortex bursting will occur as shown in Fig. 2. When vortex bursting occurs, potential theory is no longer applicable, thus requiring pressure differential measurements, $\Delta P(t)$, to obtain quantitative estimates of unsteady blade loading. At this point discussion of the experimental setup is appropriate, since it encompasses most of the problems encountered in application, such as the fact that the free-line vortex is really a well-developed tip vortex.

Experimental Apparatus

The apparatus consisted of an oscillator, situated upstream of the instrumented airfoil, capable of oscillating an airfoil (NACA 0012, Chord 7.7 in.) vertically in the spanwise direction as shown in Photograph 1. This airfoil penetrates the duct of a low turbulence wind tunnel which is described in Ref. 6. Photograph 2 shows the portion of the upstream airfoil exposed to the free stream at an angle of attack to the oncoming flow. By sinusoidally oscillating this airfoil vertically, a tip vortex is produced which will pass across the instrumented stationary airfoil (NACA 0012, Chord = 5 in.), which was mounted horizontally across the open jet portion of the duct downstream of the vertically oscillating foil. Photograph 3 shows the instrumented airfoil mounted horizontally at zero angle of attack across the test section. Photograph 4 shows the instrumented airfoil and its supporting structure situated in the open jet portion of the wind-tunnel duct.

A simplified side-view sketch in Fig. 3 shows the apparatus as a unit. The differential pressure transducer mounted 1/10 chord aft of the leading edge in the instrumented foil was of the type described in Ref. 7. With the tubular leads from the diaphram of the pressure transducer to the openings in the surface of the airfoil being somewhat lengthy, a reduction in the natural frequency to approximately 1000 Hz was estimated to occur. However, it was not possible to make a frequency-response calibration of the

pressure transducer, but only possible to do a static calibration.

The pressure transducer formed part of a bridge in a carrier amplifier system used to measure the response of the transducer. The frequency response of 5 KHz of the carrier amplifier was well above that of the transducer. However, the output of the system, due to the magnitudes of the pressures, was near the minimum with much of the signal containing a large amount of noise hash due to the carrier amplifier. To record the transient pressure signals, the carrier amplifier output was displayed on an oscilloscope and photographed using a Polaroid camera.

The experimental procedure was to run the oscillator at a nearly constant frequency of 1 Hz, with the mean position of the airfoil on the centerline of the wind-tunnel duct which is also the vertical location of the instrumented airfoil. Within the range of oscillator frequencies, which always maintained a long tip vortex wave length compared to the instrumented chord length (greater than 40) of the airfoil, the pressure response was independent of frequency (1 to 10 Hz). No pressure measurements were made with the tip vortex stationary since no accurate location of the tip vortex relative to the instrumented foil was available without smoke-flow visualization. The angle of attack of the oscillating airfoil could be set at 0°, 4°, 8°, and 12°. The downstream, instrumented foil was never given an angle of attack, but was set at one yaw-angle position of 11.3° relative to the wind-tunnel centerline. The horizontal location of the pressure transducer relative to the wind-tunnel centerline and the tip vortex was varied by horizontally sliding the foil in its mounting brackets. See Photograph 4.

The velocity of the tunnel was maintained at approximately the maximum (52 meters/sec) for the open-jet mode of operation in order to produce the largest dynamic pressures. Figure 4 shows that the pressure difference across the foil due to the vortex

interaction is directly proportional to the dynamic pressure; that is, the flow velocity squared. Also, the phase of maximum pressure is directly related to the flow velocity. This is an expected result, since the circulation of the tip-vortex generator is proportional to the flow velocity. Therefore, the induced velocity across the instrumented airfoil is proportional to the flow velocity, yielding a second power law for the pressure.

Results

Figure 5 is a plot of the maximum pressure difference across the airfoil at the 10% chord location as a function of horizontal location of the pressure transducer relative to the tunnel centerline and hence the tip vortex. These results were obtained for angles of attack of 4°, 8°, and 12° of the upstream oscillating airfoil which controlled the size of the vortex. The maximum pressures occurred in the vortex core, which does not lie exactly on the wind-tunnel centerline. A few peak pressures were plotted for which vortex bursting must have occurred in the core. These pressures are extremely sharp pulses and are very difficult to analyze. Photographs 5 through 22 are typical pressure responses for the tip vortex generator at 8° angle of attack for various spanwise locations.

Notice the large pressure differences near the core of the vortex when it passes over the foil as shown in Photographs 13 and 14. The cause of these large pressure differences is that the vortex core is bursting, causing the boundary layer to separate from the leading edge of the airfoil along a short distance of the span. See Fig. 2. In Ref. 4, photographs of this condition for the stationary tip-vortex case are shown by using smoke for flow visualization with the vortex impinging on the leading edge. Note also that the size of the vortex core does not seem to be linearly dependent upon the angle of attack of the tip-vortex generator airfoil. Separation on the upstream foil appears to be causing the

core size to remain constant above 12°. These results are more clearly explained by detailed vorticity measurements. See Figs. 6 and 7.

Figure 5 also shows the effect of yaw in reducing the maximum pressure differences occurring on the airfoil outside of the vortex core region. There appears to be more than just the influence of the cosine of yaw-angle effect on the induced velocity, since cos 11.3° = 0.962 and $\cos^2$ 11.3° = 0.925 and from Fig. 5, the yawed pressure distribution is from 16 to 23% less than that for zero yaw.

From this plot, several questions need to be answered, at least in a qualitative sense. Why does the vortex shift off of the tunnel centerline? What are the magnitudes of the peak pressures occurring in the vortex core, and what is the size of the core? Does yaw reduce the peak pressures in the vortex core?

Figure 8 is a plot of phase, which is when the occurrence of the maximum or minimum pressure difference occurs (depending on which side of the center of the vortex core the pressure transducer is located) relative to a fixed time in the cycle. The maximum pressures along the span appear to be in phase within the experimental error which appears to be about 20°. Also, the occurrence of the peak pressures inside of the core, where vortex bursting occurs, are in phase and independent of the vortex size (i.e., angle of attack of upstream airfoil). Therefore, it may be assumed that the pressure fluctuations are in phase everywhere along the span of the foil even when a small yaw angle has been introduced.

Discussion

To answer the questions posed by the analysis of the plot in Fig. 5, an examination of the wind-tunnel setup is necessary. The reason for the vortex impinging upon the downstream airfoil off centerline of the tunnel is threefold. See Fig. 9. First, the

vortex leaves the upstream foil nearer its trailing edge than on the tunnel centerline as would be predicted by linear airfoil theory. Second, the vortex is displaced as it rolls up both vertically and horizontally. Third, the vortex moves horizontally as it impinges upon the downstream airfoil, due to the image vortex created by the solid boundary of the wing.

The two possible angles of attack of the tip vortex generator airfoil are shown. We see that the vertical effect of rollup is the same for both + and - angles of attack. Since the mean position of the oscillating airfoil was the tunnel centerline, all of the pressure signals were not symmetric in time since the vortex traveled a greater distance below the downstream airfoil than above it. In future tests this could be adjusted by raising the mean position of the oscillating airfoil above the downstream airfoil, thus accounting for wake rollup in the spanwise direction or as in this setup, in the vertical direction.

The effect of the rigid surface of the downstream foil requiring an image vortex to balance the normal velocity induces a horizontal velocity in the tip vortex as it approaches the foil. Its effect is a 180° phase shift in the location of the vortex path relative to the airfoil for + or - angles of attack of the oscillating airfoil. However, no estimates could be made of the overall vortex change in location when crossing the foil in opposite directions. It would appear that this distance d (see Fig. 9) would be small at the leading edge, but flow visualization would be needed to verify this.

A consistency was maintained in the measurement of phase and maximum amplitude in that the phase was referenced to the time when the oscillating airfoil passed the mean position traveling in the down direction. All three causes of shift in vortex location are related to the flow velocity indicating why the phase in Fig. 4 varied directly with the flow velocity.

RC

Various methods of estimating rollup of the vortex wake were made using methods listed in Ref. 4, but about the only conclusion which could be made is that the vortex wake was completely rolled up, which is to say that the upstream oscillating airfoil was far enough away from the downstream airfoil. This was verified by the repeatability of the pressure signal throughout the experiment. Estimates for vortex core shift produced meaningless results, since the experimental apparatus was surrounded by the four duct walls of the 15 in. x 15 in. test section, and no present theory considers the wall effect on the wake. Another aspect of the problem not considered is the fact that the oscillating, upstream foil has an oscillating aspect ratio, since it penetrates the tunnel duct wall.

To determine experimentally the pressure difference when vortex bursting occurs will require two improvements to the present setup. First, the frequency response of the recording system must be very high in order to respond to the impulse-type pressures as shown in Photograph 13. Also, since the core size appears to be extremely small relative to the overall size of the vortex, a very precise traversing mechanism is needed in order to position the pressure transducer relative to the core. A means to visualize the vortex as it impinges upon the foil would be beneficial in demonstrating repeatability of the setup and in allowing possible stationary vortex measurements. The biggest problem is in the interpretation of this impulsive pressure. No one but Leverton [Ref. 3] considers the cause of this impulsive pressure, and he examines the case of the vortex appearing as a gust on the airfoil. His approach is not applicable to this experiment because the vortex considered has its axis parallel to the span of the airfoil and not perpendicular to it.

The effect of yaw on the peak pressure seems to have the same effect inside the core of the vortex as well as outside the core in reducing the pressure difference. Comparing Photograph 23

to Photograph 14 for pressure transducers located on the centerline, and Photograph 24 to Photographs 18 or 10 for pressure transducers located 1 in. off the centerline, there is no difference in the wave form of the patterns or in phase shift as indicated in Fig. 8.

The velocity distribution of the line vortices plotted in Fig. 7 has been converted to a dynamic pressure distribution and plotted in Fig. 10. If these stagnation pressures in Fig. 10 are compared to the peak pressure differences at the 10% chord of Fig. 5, the maximum peak pressures for the vortex cases created by the vortex tip generator at $\alpha = 4$ and $8°$ appear to be twice the dynamic pressure of the vortex core, and about the same value for $\alpha = 12°$. However, if the vortex core velocity given in Fig. 7 is considered as a spanwise distribution of downwash, in a quasi-steady sense as done in Refs. 4 and 8, then the region inside of the core would be separated along the span. The result of these high velocities compared to free stream is to cause the separation on the airfoil to spread out along the span. This effect and the induced horizontal velocity of the vortex as it approaches the airfoil cause the peak pressure differences to spread out across the span. This can be seen by comparing Fig. 5 to Figs. 7 and 10.

Conclusions

The maximum pressures occurring because of vortex interaction act in phase along the span of the airfoil even with the introduction of yaw. The phase (time to maximum pressure difference) appears to be directly proportional to the flow velocity and hence the circulation of the impinging vortex.

The absolute values of maximum pressures seem to be directly proportional to the flow velocity squared or the dynamic pressure of the flow. Therefore the maximum pressures should also be proportional to the circulation squared of the impinging vortex.

Yaw angle tends to considerably diminish the maximum pressures inside of the vortex core where bursting takes place, and also has the same effect outside the core.

The maximum dynamic pressure coefficient $\Delta p(t)/(1/2\rho U^2)$ are as high as 0.5 with peak dynamic pressure coefficients possibly as high as 1.0.

REFERENCES

1. Loewy and Sutton. "A Theory for Predicting the Rotational Noise of Lifting Rotors in Forward Flight." US AAV LABS TR 65-82, Jan. 1966.

2. Schlegel, King, and Mull. "Helicopter Rotor Noise Generation and Propagation." USAAV LABS, TR 66-4, Oct. 1966.

3. Leverton, J.W. "Helicopter Noise-Blade Slap." NASA CR-1221, Oct. 1968.

4. Silver, L.W. "An Investigation of the Interaction of a Trailing Vortex with a Lifting Surface." S.M. Thesis, Dept. of Aeronautics and Astronautics, M.I.T., June 1967.

5. Curle, N. "The Influence of Solid Boundaries upon Aerodynamic Sound." Proc. Royal Society London, A231, 505-514, 1955.

6. Hanson, C.E. "Design and Construction of a Low Speed Wind Tunnel." Acoustics and Vibrations Lab. Rept. No. 79611-1, Engineering Projects Lab., M.I.T., Feb. 1969.

7. Patterson, J.L. "A Miniature Electrical Pressure Gage Utilizing a Stretched Flat Diaphram." NACA TN 2659, April 1952.

8. Simons, I.A. "Blade-Vortex Interaction on Helicopter Rotors in Forward Flight." Institute of Sound and Vibration, Southampton, Memorandum ISAV 126, July 1965.

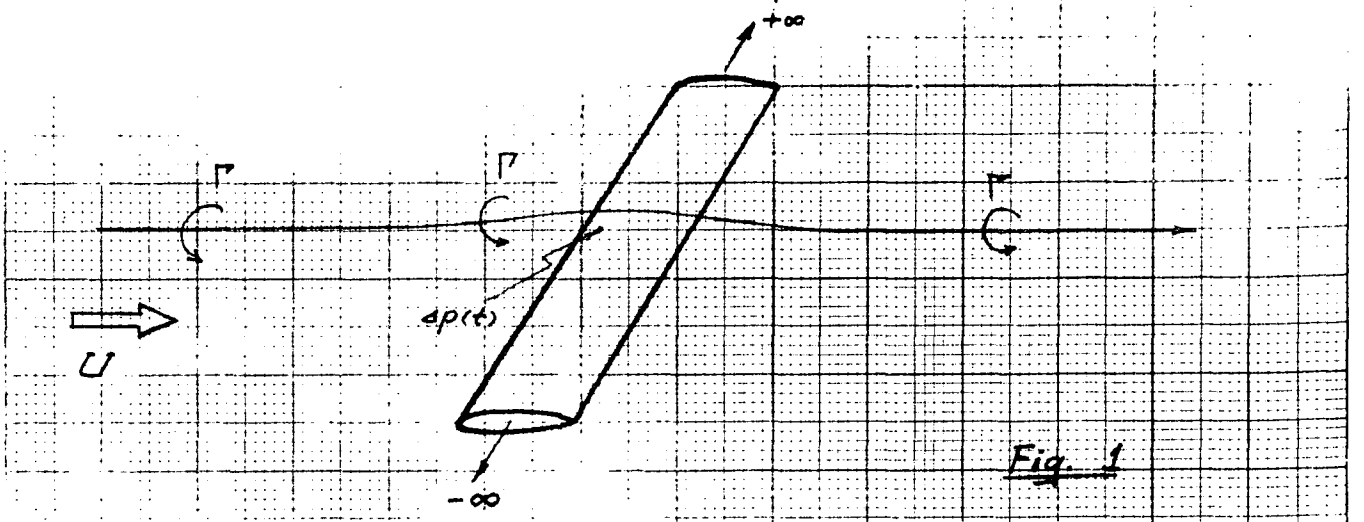

Fig. 1

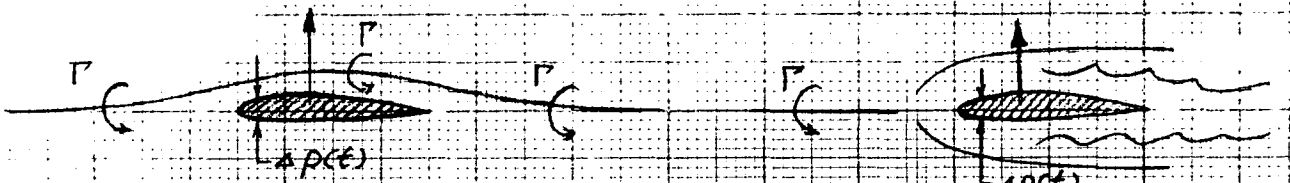

Foil Rising into Vortex

Vortex Bursting

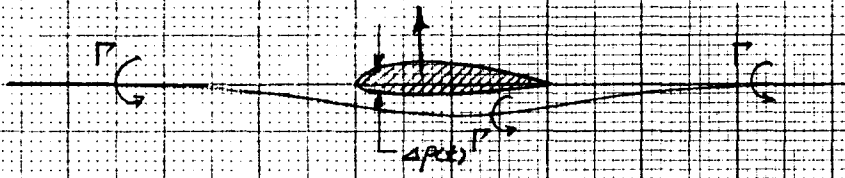

Foil Passing out of Vortex

Fig. 2

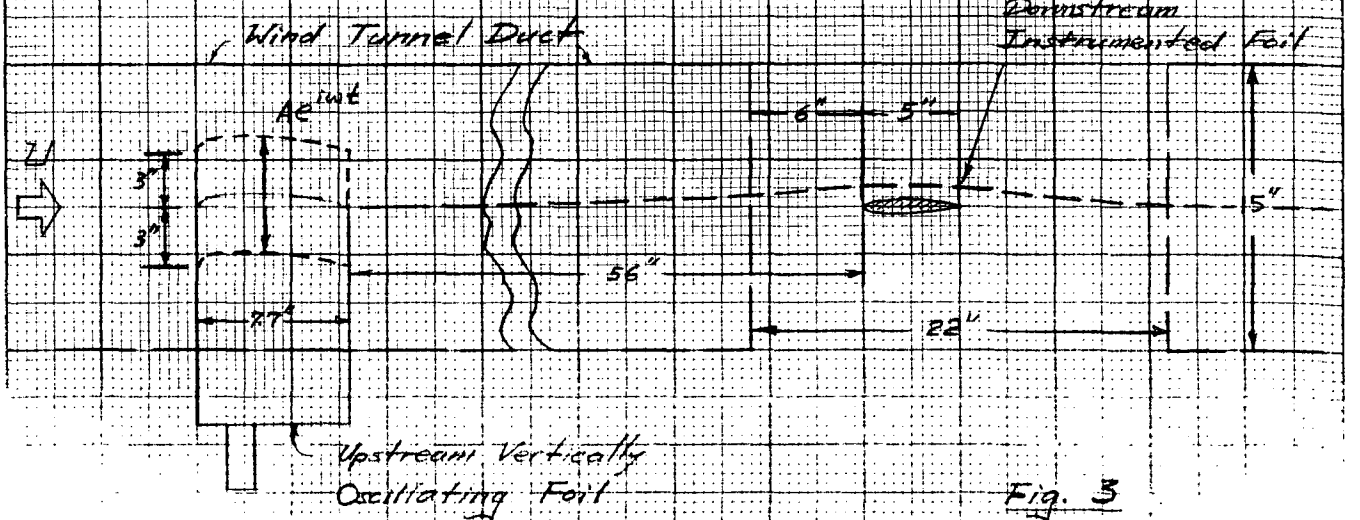

Fig. 3

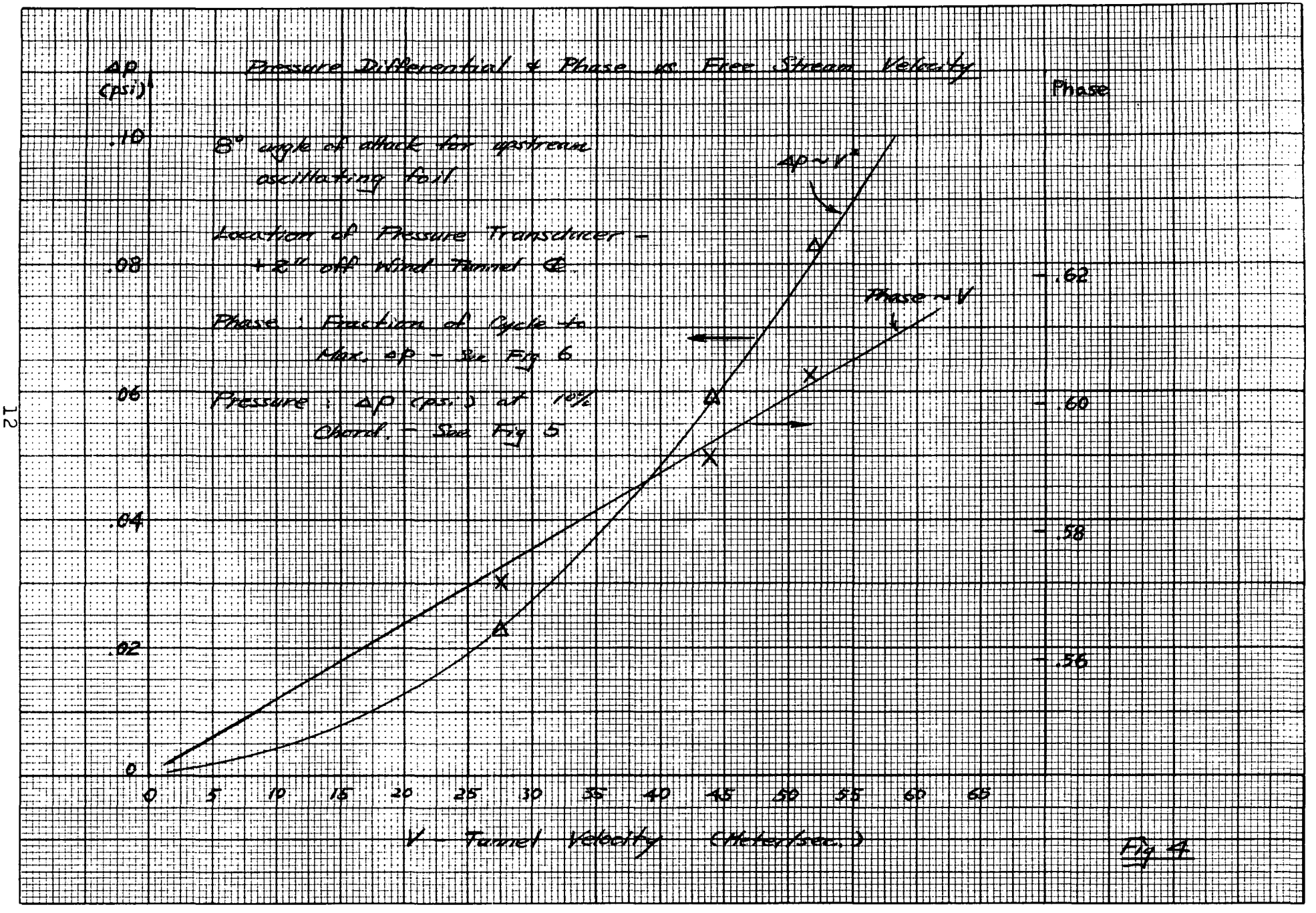
Pressure Differential & Phase vs Free Stream Velocity
ΔP (psi)
Phase
.10
.08
.06
.04
.02
0
-.62
-.60
-.58
-.56
0 5 10 15 20 25 30 35 40 45 50 55 60 65
V - Tunnel Velocity (Meters/sec.)
8° angle of attack for upstream oscillating foil
Location of Pressure Transducer - +2" off Wind Tunnel ℄
Phase : Fraction of Cycle for Max. ΔP - See Fig 6
Pressure : ΔP (psi.) at 10% Chord. - See Fig 5
ΔP ~ V²
Phase ~ V

Fig 4

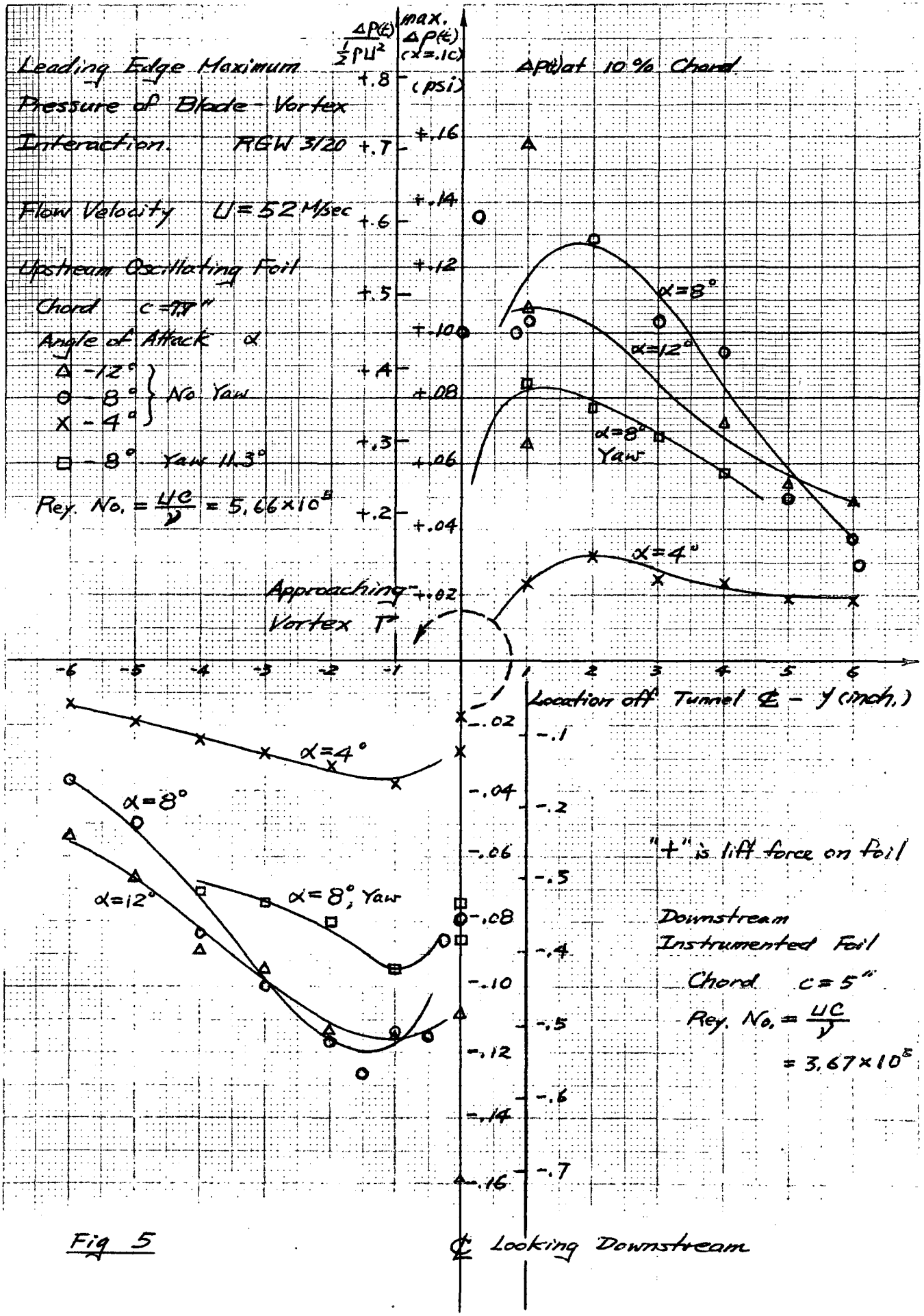
Leading Edge Maximum Pressure of Blade-Vortex Interaction. RGW 3/20
Flow Velocity U = 52 M/sec
Upstream Oscillating Foil
Chord c = 7.5"
Angle of Attack α
△ -12°
○ -8°
× -4°
} No Yaw
□ -8° Yaw 11.3°
Rey. No. = Uc/ν = 5.66×10^5
Δp(t)/½ρU²
max. Δp(t) (x=.1c) (psi)
Δp(t) at 10% Chord
α=8°
α=12°
α=8° Yaw
α=4°
Approaching Vortex
Location off Tunnel ℄ - y (inch.)
α=4°
α=8°
α=12°
α=8°, Yaw
"+" is lift force on foil
Downstream Instrumented Foil
Chord c = 5"
Rey. No. = Uc/ν = 3.67×10^5
℄ Looking Downstream

Fig 5

Vorticity Distribution of Upstream Oscillating Airfoil in Stationary Position Tip Located on Tunnel ℄

$\omega = 2\pi f$ (rad/sec)

$\xi = 2\omega$
$= 4\pi f$ (rad/sec)

$\Gamma(r) = \int \vec{\xi} \cdot d\vec{A}$
$= 2\pi \int_0^r \xi\, r_1\, dr_1$
$= 8\pi^2 \int_0^r f(r_1)\, r_1\, dr_1$

$u(r) = \frac{\Gamma(r)}{2\pi r}$
$= \frac{4\pi}{r} \int_0^r f(r_1)\, r_1\, dr_1$

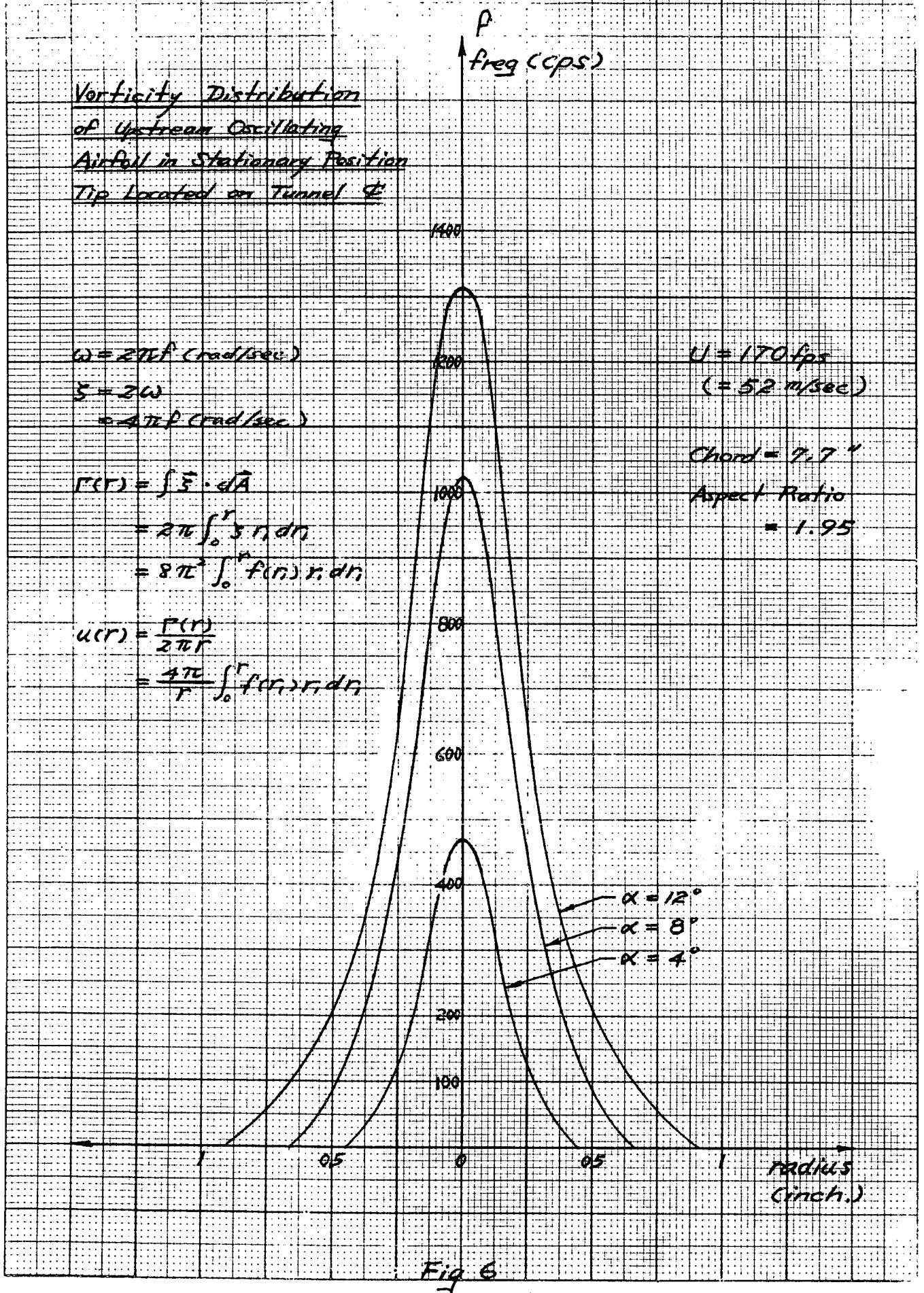

$U = 170$ fps
$(= 52$ m/sec$)$

Chord $= 7.7$"

Aspect Ratio
$= 1.95$

Fig 6

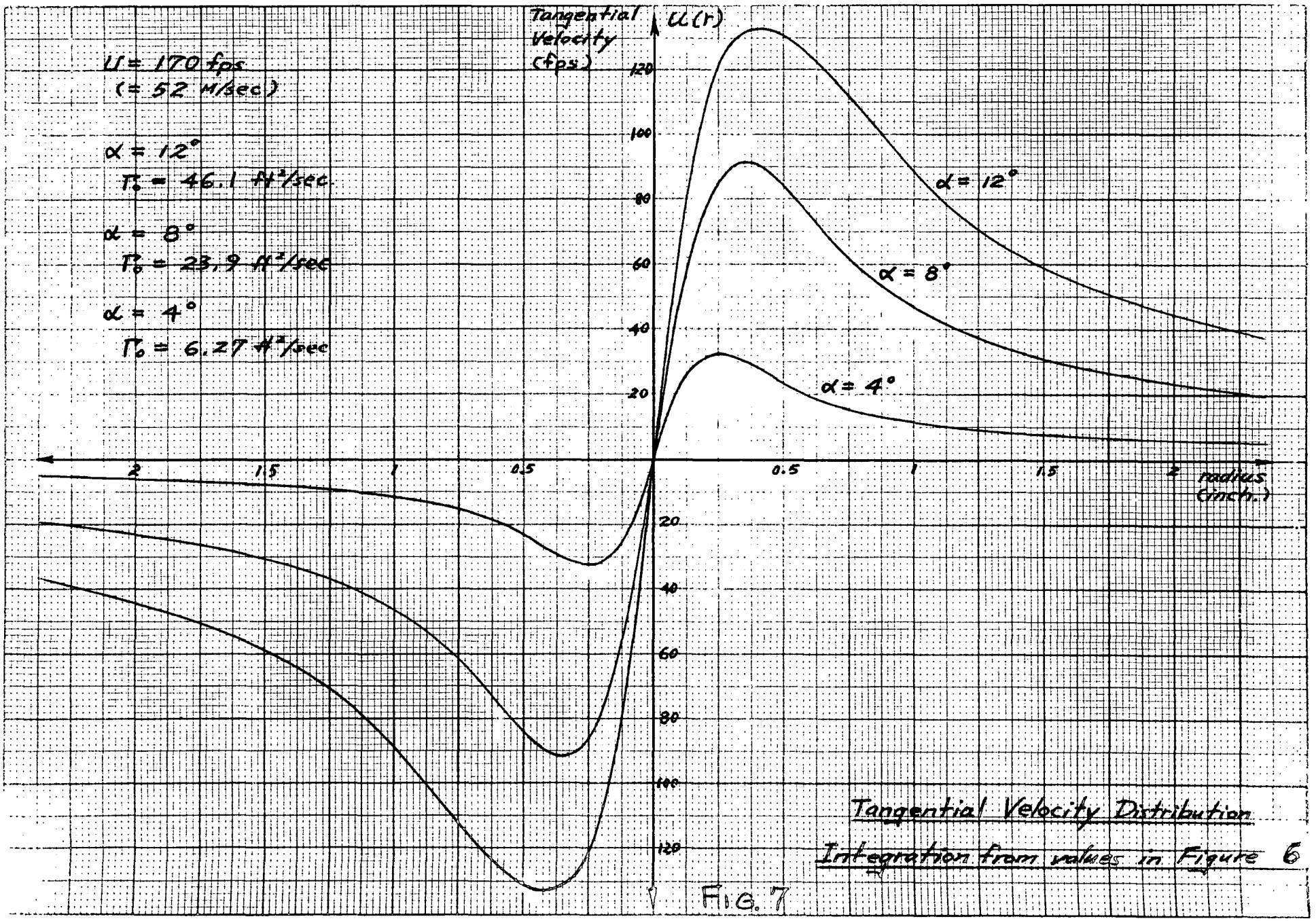

Tangential Velocity Distribution

Integration from values in Figure 6

F.G. 7

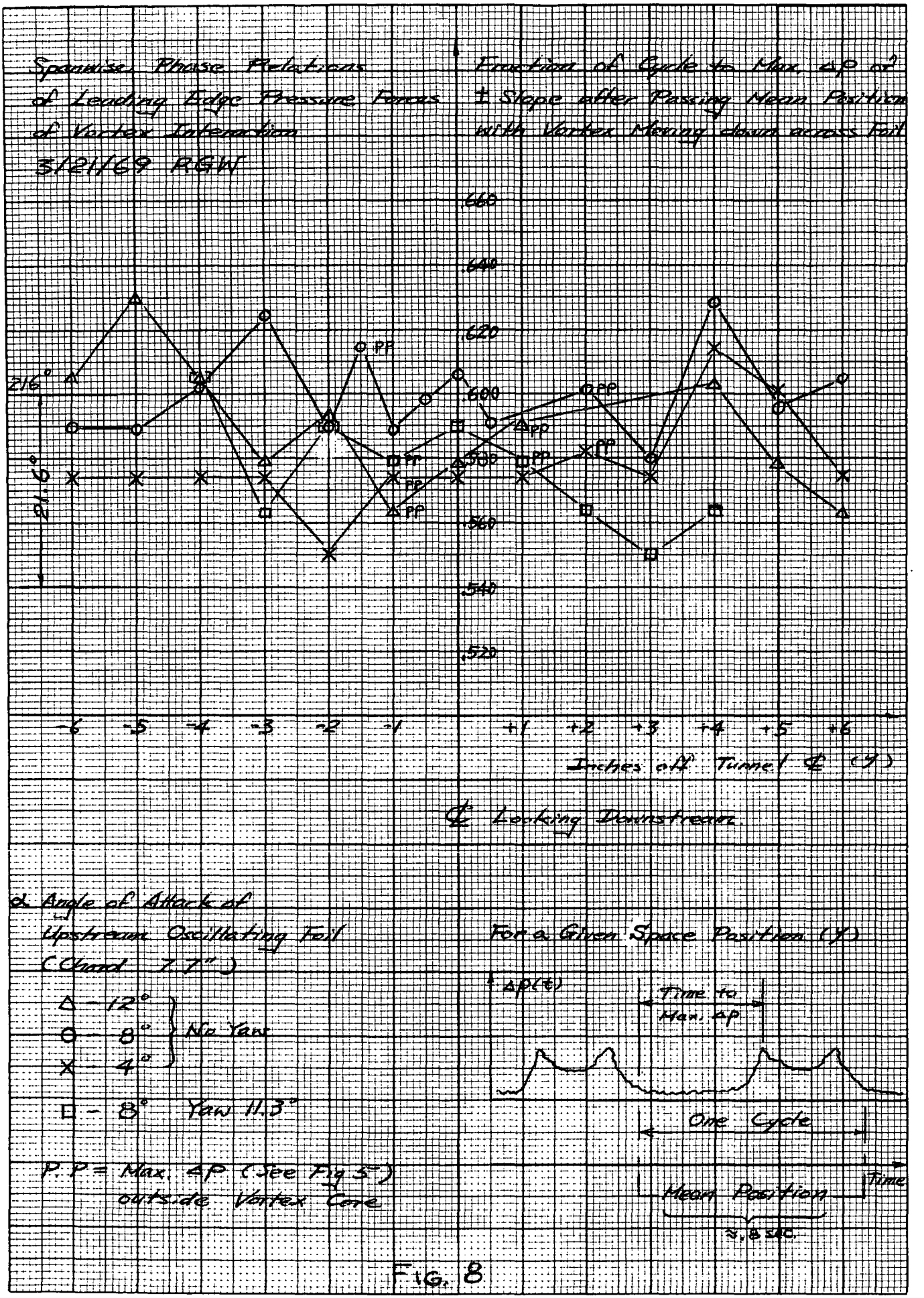
Spanwise Phase Relations of Leading Edge Pressure Forces & Vortex Interaction
3/21/69 RGW
Fraction of Cycle to Max. Δp or ± Slope after Passing Mean Position with Vortex Moving down across foil
660
640
620
600
580
560
540
520
216°
φ
PP
-6 -5 -4 -3 -2 -1 +1 +2 +3 +4 +5 +6
Inches off Tunnel ℄ (y)
℄ Looking Downstream
α Angle of Attack of Upstream Oscillating Foil (Chord 7.7")
Δ - 12°
O - 8°
X - 4°
} No Yaw
□ - 8° Yaw 11.3°
P.P = Max. Δp (see Fig 5) outside Vortex Cone
For a Given Space Position (y)
± Δp(t)
Time to Max. Δp
One Cycle
Mean Position
Time
≈.8 sec.

Fig. 8

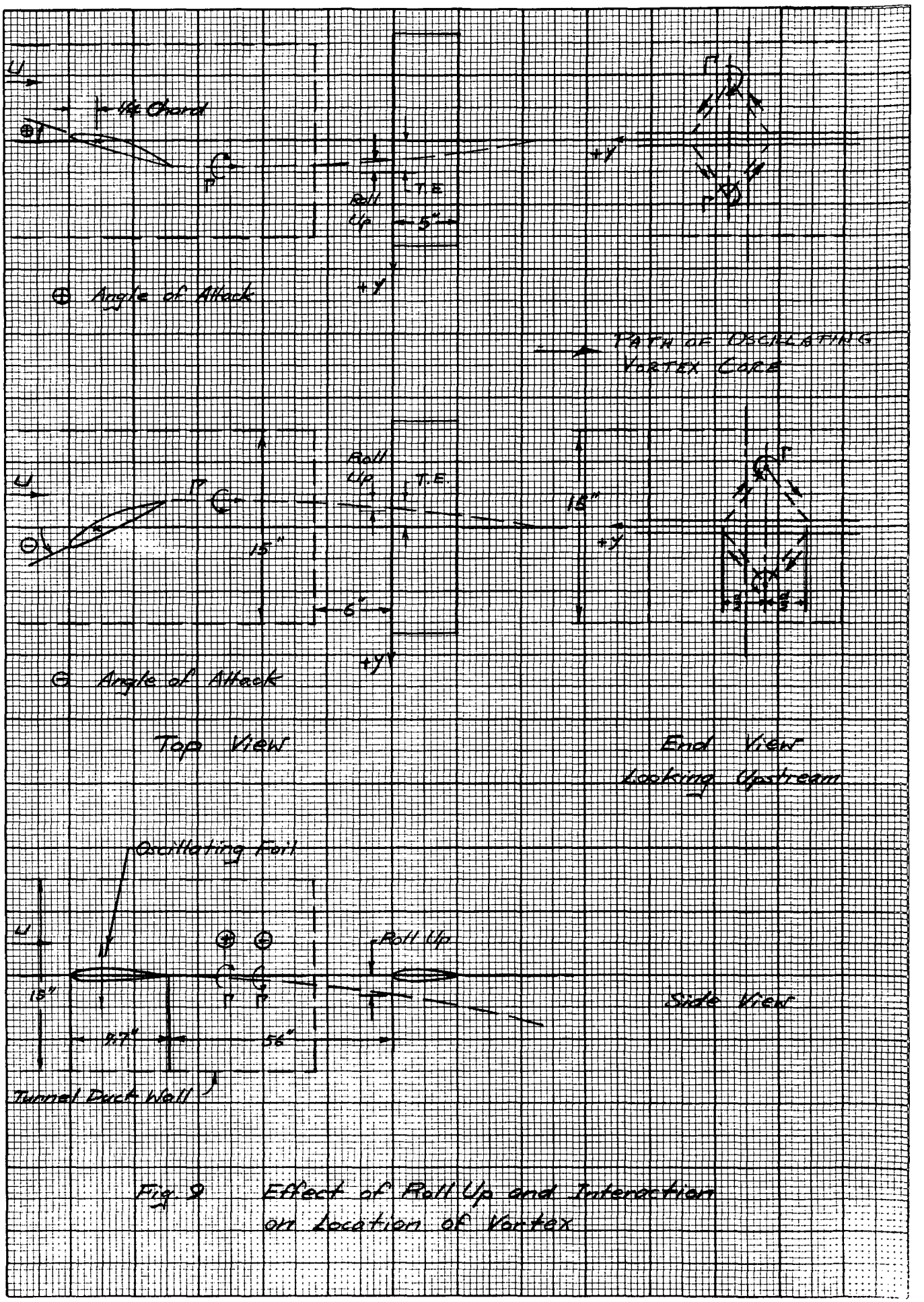

Fig. 9 Effect of Roll Up and Interaction on Location of Vortex

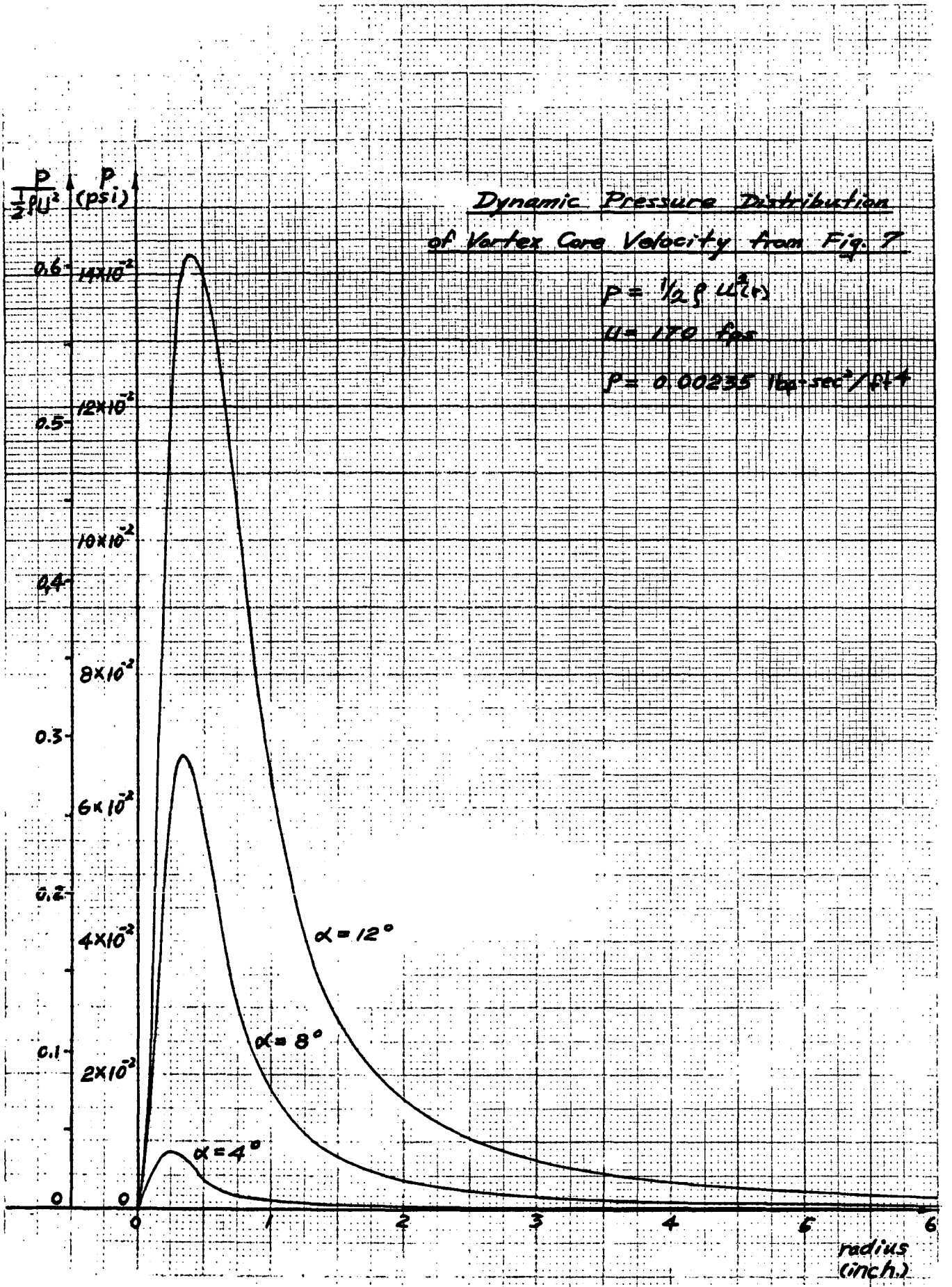
Dynamic Pressure Distribution
of Vortex Core Velocity from Fig. 7
$p = \frac{1}{2}\rho u^2(r)$
$u = 170$ fps
$\rho = 0.00235$ lbf-sec^2/ft^4
$\frac{p}{\frac{1}{2}\rho U^2}$
p (psi)
0.6
14×10^{-2}
0.5
12×10^{-2}
10×10^{-2}
0.4
8×10^{-2}
0.3
6×10^{-2}
0.2
4×10^{-2}
0.1
2×10^{-2}
0
0
$\alpha = 12°$
$\alpha = 8°$
$\alpha = 4°$
0
1
2
3
4
5
6
radius (inch.)

Fig. 10

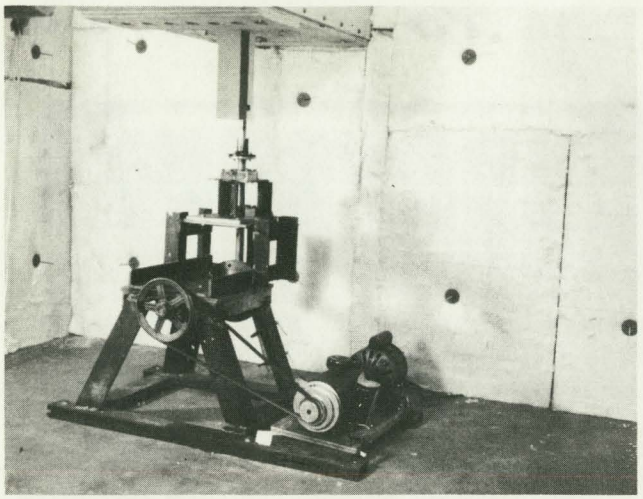

No. 1 Upstream Airfoil + Oscillator.

No. 2 Upstream Airfoil in Wind Tunnel Duct Looking Upstream.

Reproduced from best available copy.

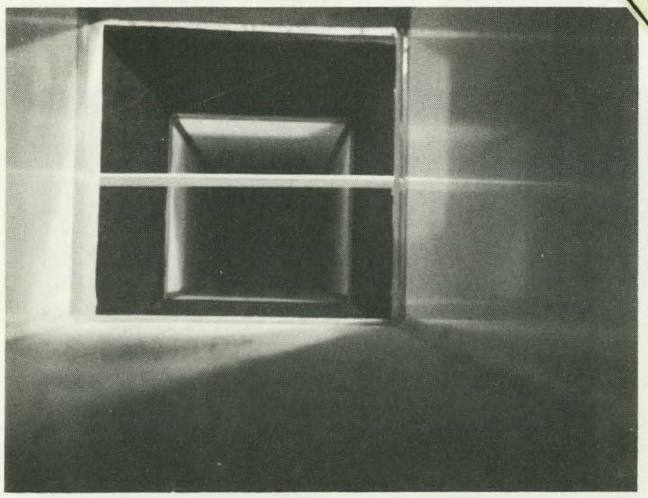

No. 3 Instrumented Airfoil Mounted across Open Jet Test Section Looking Downstream.

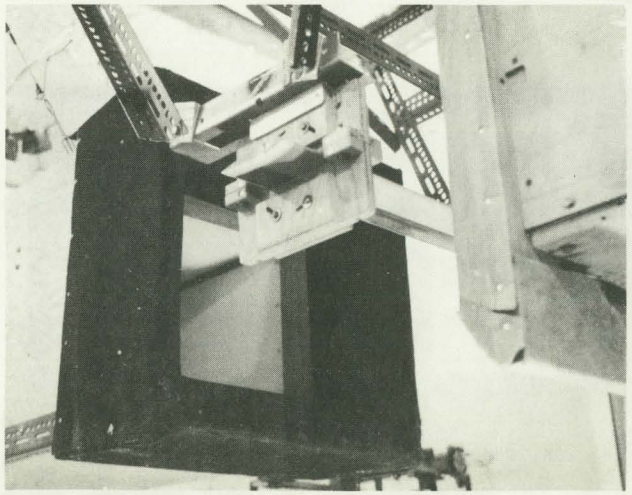

No. 4 Instrumented Airfoil Mounted in Open Jet Test Section.

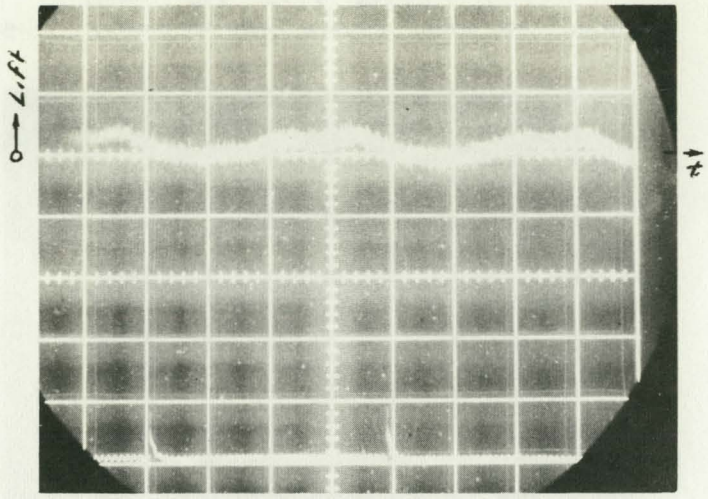

No. 5 $y = 6''$, $\alpha = 8°$
SR = .2 sec/cm, psi/cm = .063

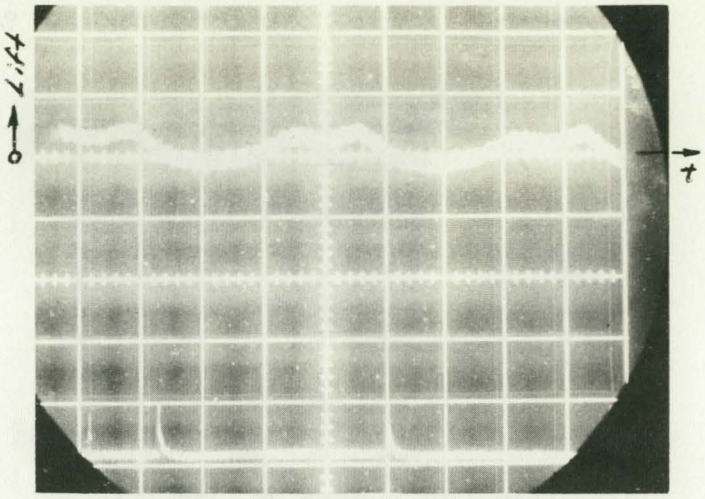

No. 6 $y = +5''$, $\alpha = 8°$
SR = .2 sec/cm. psi/cm. = .063

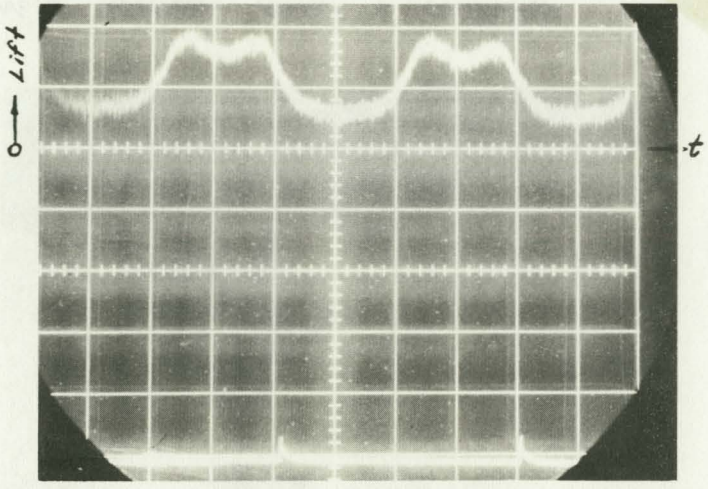

No. 7 $y = +4''$ $\alpha = 8°$
SR = .2 sec/cm. psi/cm. = .056

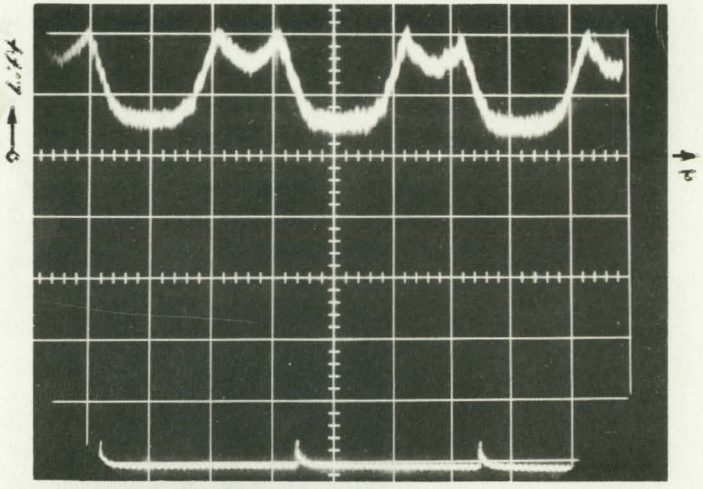

No. 8 $y = +3''$ $\alpha = 8°$
SR = .2 sec/cm. psi/cm. = .056

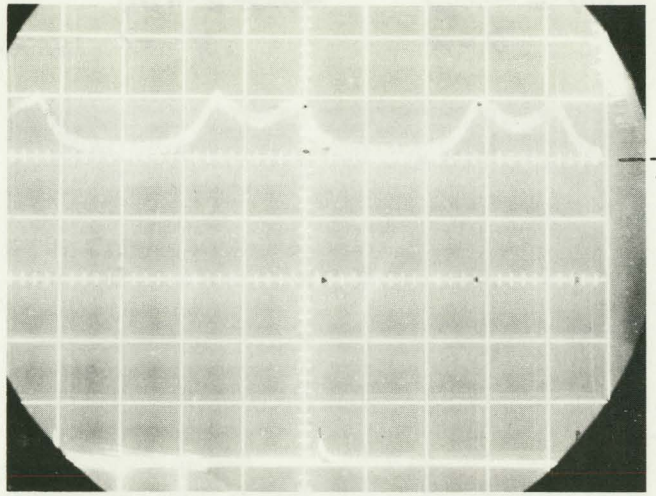

No. 9 $y = +2''$ $\alpha = 8°$
SR = .2 sec/cm psi/cm = .107

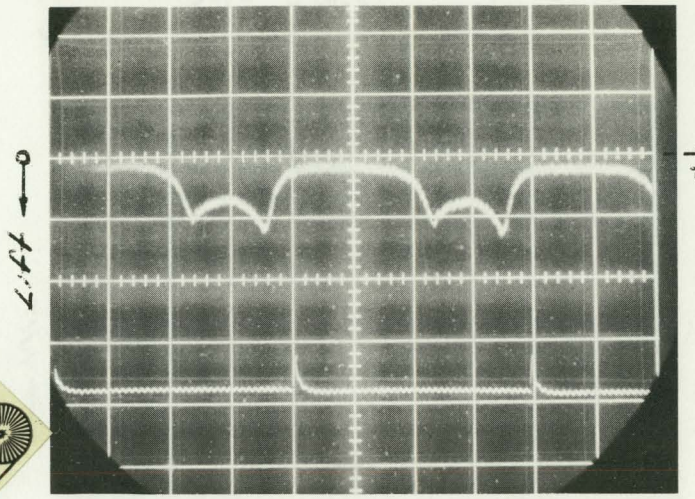

No 10. $y = +1''$ $\alpha = 8°$
SR = .2 sec/cm. psi/cm = .105

Reproduced from best available copy.

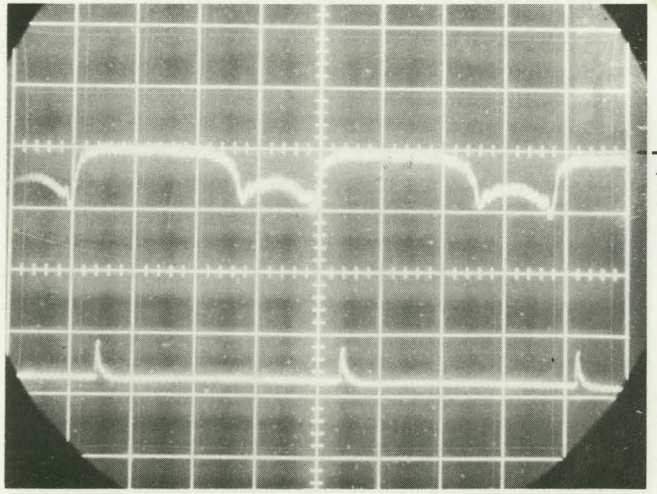

No. 11 $y = +3/4''$ $\alpha = 8°$
SR = .2 sec/cm. psi/cm = .105

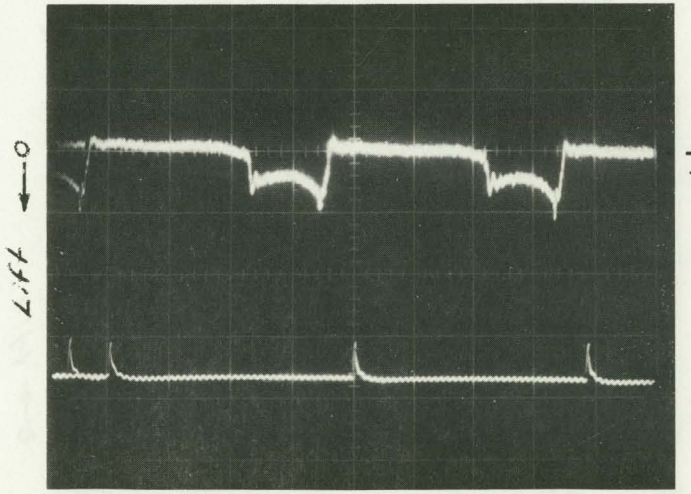

No 12. $y = +\frac{1}{2}''$ $\alpha = 8°$
SR = .2 sec/cm. psi/cm = .105

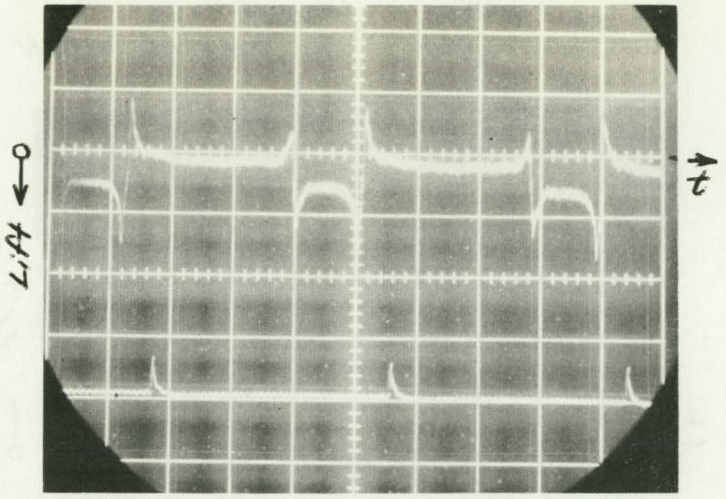

No. 13 $y = +\frac{1}{4}$" $\alpha = 8°$
SR = .2 sec/cm. psi/cm = .105

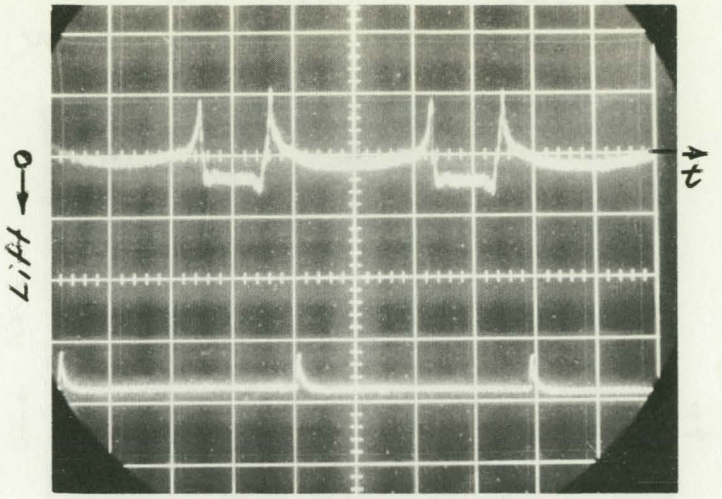

No. 14. $y = 0$" $\alpha = 8°$
SR = .2 sec/cm. psi/cm = .105

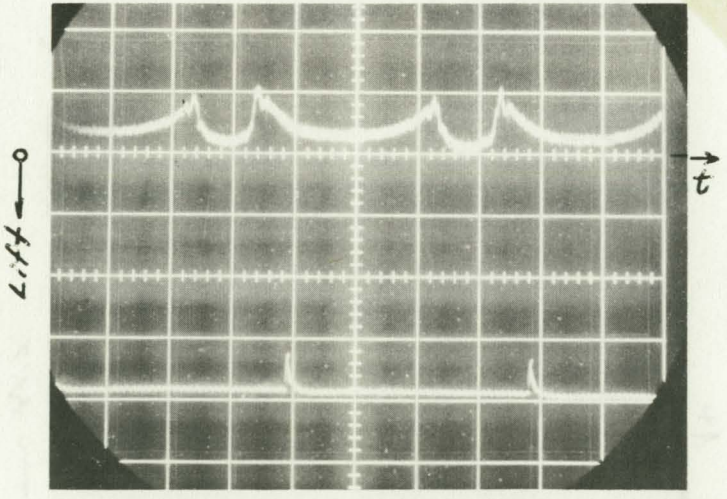

No. 15. $y = -\frac{1}{4}$" $\alpha = 8°$
SR = .2 sec/cm. psi/cm = .105

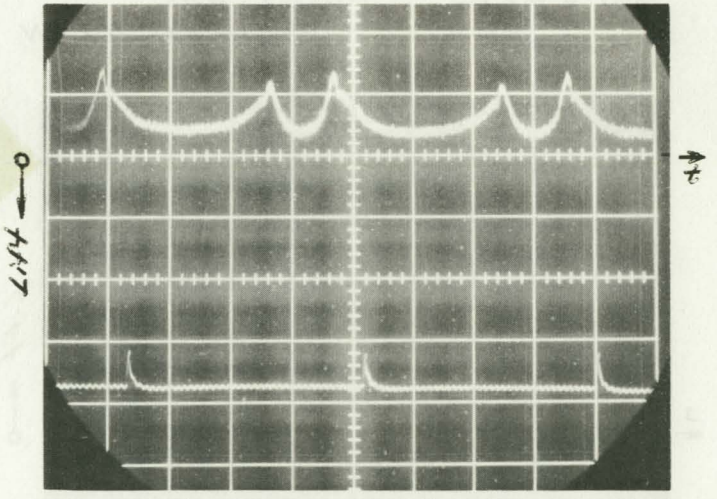

No. 16. $y = -\frac{1}{2}$" $\alpha = 8°$
SR = .2 sec/cm. psi/cm = .105

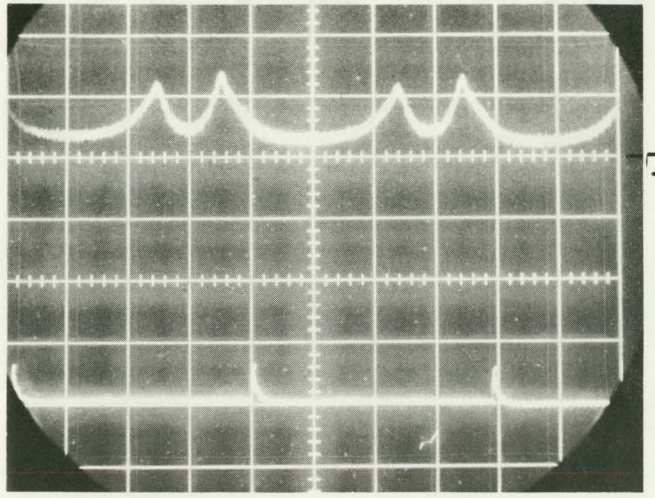

No. 17 $y = -3/4''$ $\alpha = 8°$
SR = .2 sec/cm. psi/cm = .105

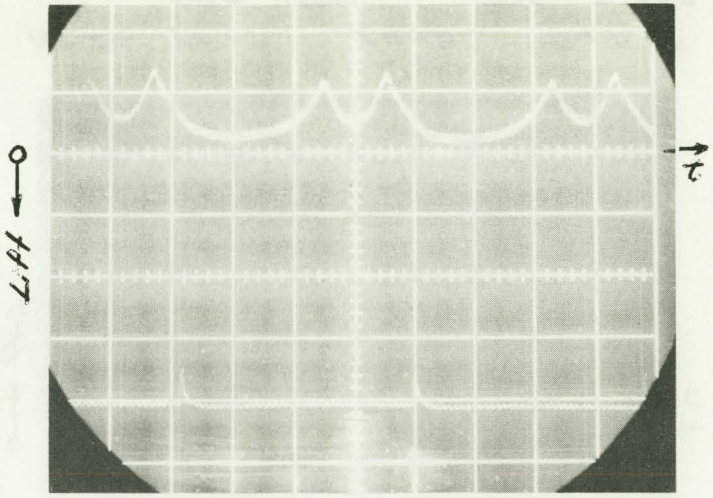

No. 18 $y = -1''$ $\alpha = 8°$
SR = .2 sec/cm. psi/cm = .105

Reproduced from best available copy.

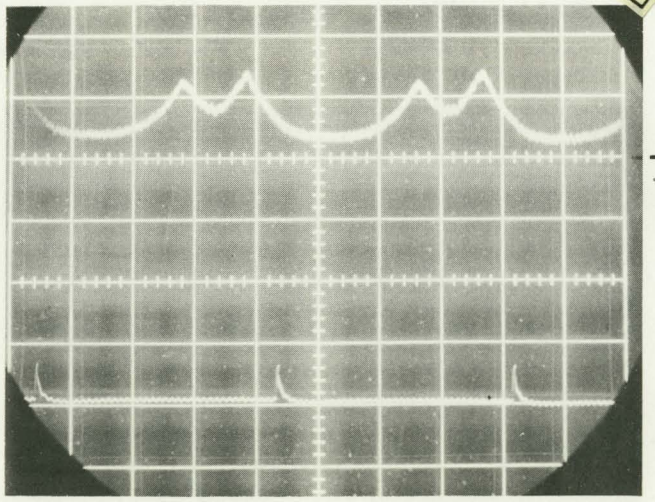

No. 19 $y = -1\frac{1}{2}''$ $\alpha = 8°$
SR = .2 sec/cm. psi/cm = .105

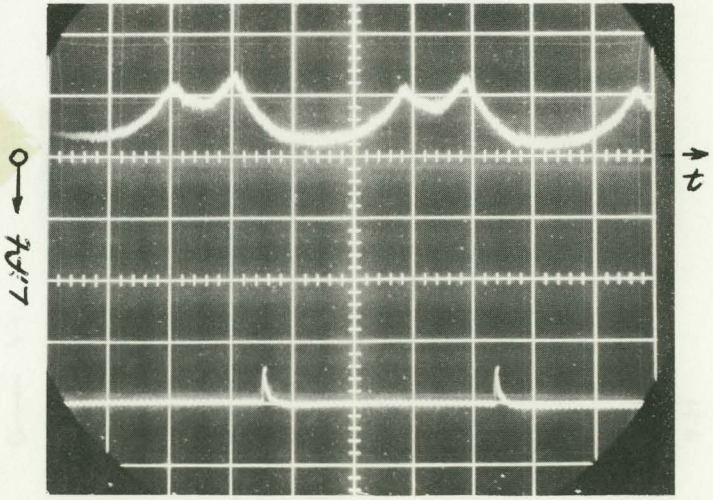

No. 20 $y = -2''$ $\alpha = 8°$
SR = .2 sec/cm. psi/cm = .105

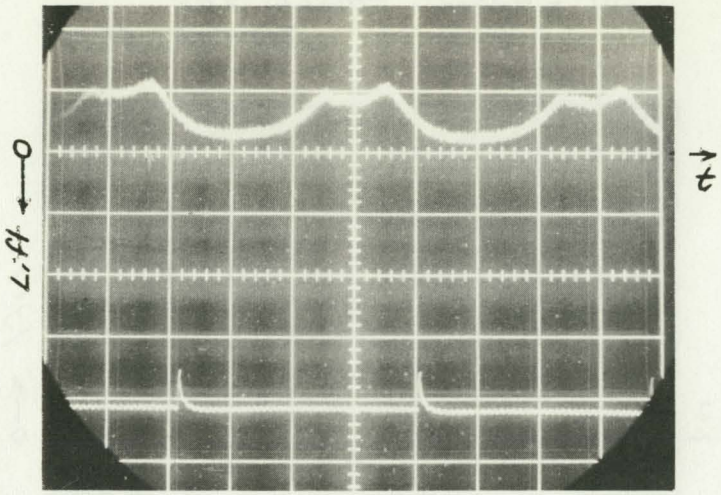

No. 21 $y = -3''$ $\alpha = 8°$
SR = .2 sec/cm. psi/cm. = .105

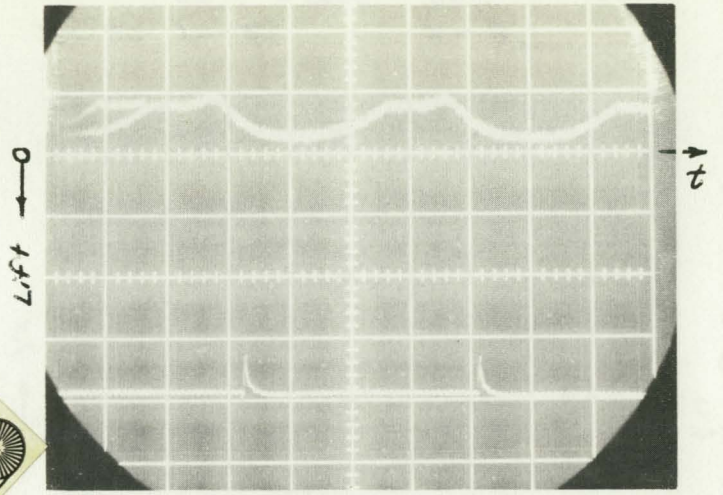

No. 22 $y = -4''$ $\alpha = 8°$
SR = .2 sec/cm psi/cm = .105

Reproduced from best available copy.

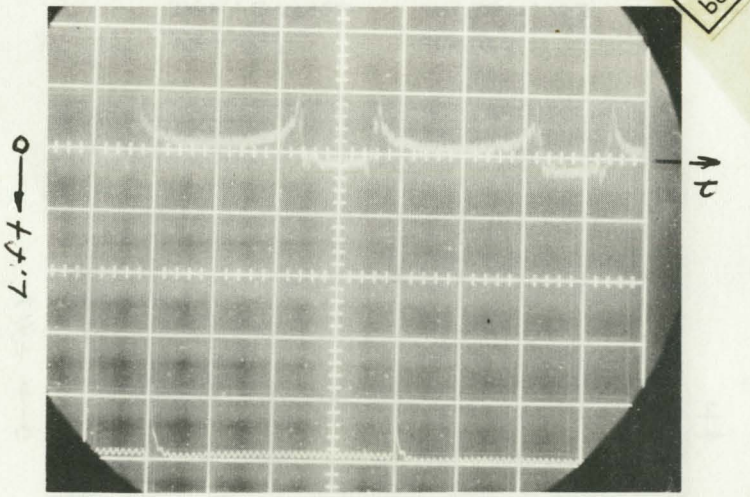

No. 23 $y = 0''$ $\alpha = -8°$ Yaw 11.3°
SR = .2 sec/cm. psi/cm = .060

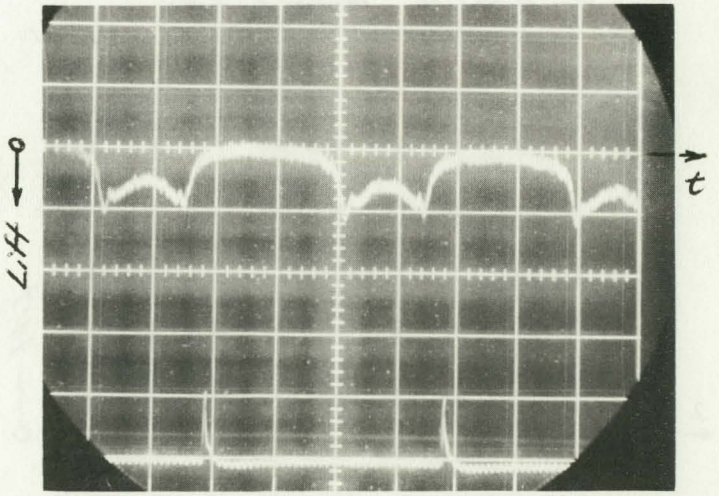

No. 24 $y = -1''$ $\alpha = -8°$ Yaw 11.3°
SR = .2 sec/cm. psi/cm = .060